Nickel ferrite/polypyrrole core-shell composite as an efficient electrode material for high-performance supercapacitor

Cite as: AIP Advances **9**, 055218 (2019); https://doi.org/10.1063/1.5090310
Submitted: 26 January 2019 • Accepted: 07 May 2019 • Published Online: 21 May 2019

Sacchidanand S. Scindia, Ramesh B. Kamble and Jayant A. Kher

Nickel ferrite/polypyrrole core-shell composite as an efficient electrode material for high-performance supercapacitor

Cite as: AIP Advances 9, 055218 (2019); doi: 10.1063/1.5090310
Submitted: 26 January 2019 • Accepted: 7 May 2019 •
Published Online: 21 May 2019

Sacchidanand S. Scindia,[1,a)] Ramesh B. Kamble,[2] and Jayant A. Kher[1]

AFFILIATIONS

[1] Department of Applied Sciences, Govt. College of Engineering Pune 411005, Maharashtra, India
[2] Department of Physics, Govt. College of Engineering Pune 411005, Maharashtra, India

[a)] Corresponding author: shrivigraha@gmail.com

ABSTRACT

In the present work, we report the high-performance supercapacitive behavior of NFO/PPy core–shell composite. The composite electrode was prepared by adopting simple and inexpensive *in-situ* chemical oxidation route in an aqueous medium containing sodium dodecyl sulfate (SDS) as a surfactant and characterized for the spectral, structural, electrical, thermal and morphological studies. The electrochemical properties were recognized by cyclic voltammetry, charge–discharge and electrochemical impedance spectroscopy. The supercapacitive performance of NFO/PPy electrode was studied in an aqueous 0.1N H_2SO_4 electrolyte solution. The effect of electrolyte concentration on specific capacitance and the stability of electrode were studied. The highest specific capacitance (C_s) achieved with NFO/PPy electrode was 721.66 Fg^{-1}. The specific energy (E_s), specific power (P_s) and coulomb efficiency (η%) were observed to be 51.95 $Whkg^{-1}$, 6.18 $kWkg^{-1}$ and 99.08% respectively. This electrode shows the outstanding electrochemical stability over 1000th continuous charging–discharging cycles and emerged as an efficient electrode material for energy storage devices as a supercapacitor.

I. INTRODUCTION

Supercapacitors act as transitional structures that link the energy gap between high power output and high energy-storage.[1] They have high energy density, stability and high efficiency toward the charging and discharging cycles. Therefore, it is essential to fabricate and improve the electrode material with high performance, low cost, and ecofriendly power sources applications. Hence, supercapacitor study has received more attention of researchers due to the potential applications as energy-storage and exchange system.[2,3] Nickel ferrite (NFO) has spinel structure based on a face centered cubic lattice of the oxygen ions with the unit cell consisting of eight formula units. The tetrahedral sites (A) and the octahedral sites (B) are occupied by metallic cations in the unit cell.[4] It is an inverse spinel ferrite having structural formula $(Fe^{3+})[Ni^{2+}Fe^{3+}]O_4$. In inverse spinel structure, the Ni^{2+} ions together with half of the Fe^{3+} ions occupy B-sites and remaining half of the Fe^{3+} ions reside in tetrahedral A-sites. The electrical, structural and magnetic properties of NFO are dependent on magnetic interaction and distribution of cations among tetrahedral (A) and octahedral (B) sites.[5] NFO reveals the variation of electrical, magnetic and electrochemical properties dependent on their crystal structure and cation distribution.[6]

In general, transition metal oxides and highly porous activated carbon materials are used as the electrode materials for electric double-layer capacitors[7] as well as supercapacitors.[8] The activated carbon shows high specific capacitance, but poor conductivity and micro porous nature which usually affects its performance.[9,10] Therefore, since few decades, transition metal oxides[11] and some ferrites[12] have been used as favorable electrode materials for supercapacitor applications due their high specific capacitance. Bhojane et al.[13] reported that the template free synthesis of NFO nanostructure electrode for supercapacitor with highest specific capacitance of 541 Fg^{-1} at the scan rate of 2mVs^{-1}. Venkatachalam et al.[14] reported

the maximum capacitance of 454 Fg^{-1} using nickel ferrite electrode synthesized through combustion route. Hareesh et al.[15] reported PEDOT:PSS wrapped $NiFe_2O_4$/rGO tertiary nanocomposite and GNP showed specific capacitance of 1090 Fg^{-1} at the scan rate of 0.5 Ag^{-1}. Sahoo et al.[16] reported a facile non-templated hydrothermal synthesized of nickel ferrite/carbon nanotube composites. Oguntoye et al.[17] obtained specific capacitance of 970 Fg^{-1} at 2 Ag^{-1} for binder-Free Nickel cobaltite based supercapacitor electrode over 3000 charge-discharge cycles.

NFO electrode is generally magnetic but electrically resistive material and polypyrrole (PPy) is a conducting polymer. But NFO/PPy core–shell composites are magnetic as well as electrically conducting. Therefore NFO/PPy core–shell is considered as a potential electrode material due to its excellent reversible redox behavior. The present work is focused on novel cost-effective synthesis of PPy with spinel ferromagnetic material such as nickel ferrite to form NFO/PPy core–shell composite. The electrochemical behavior of the core–shell composite was studied by cyclic voltammetry; galvanostatic charge–discharge techniques confirmed the electro activity as well as supercapacitive performance of the composite electrode. To the best of author knowledge, there is no report found on NFO/PPy core–shell electrode for supercapacitor applications.

II. EXPERIMENTAL DETAILS

A. Materials and chemicals

Pyrrole (Aldrich) was purified by vacuum distillation before use. The metal salts of ferric nitrate $Fe(NO_3)_3$ $6H_2O$ (99%), nickel nitrate $Ni(NO_3)_2$ $6H_2O$ were used as metal precursors. Citric acid, ethyl alcohol, sodium dodecyl sulfate (SDS), sodium hydroxide and cetryl trimethyl ammonium bromide were obtained from commercial suppliers and used as received. All chemicals were of analytical reagent grade.

B. Preparation of sole–gel auto combustion assisted simple $NiFe_2O_4$ spinel ferrite material

For the typical synthesis, the stoichiometric quantities of metal nitrate, ferric nitrate hexahydrate (2M) and of citric acid (1M) were dissolved in 100 mL of deionized water separately. The molar ratio of nitrates to citric acid was maintained as 1:1. The separate solutions were mixed together and the pH value of mixture was adjusted to 7 by adding CTAB buffer solution. Then the mixed solution was kept stirred at 100°C for the dehydration reaction. After dehydration, viscous gel was formed. Subsequently, the gel solution was undergoing self-ignition at around 300°C. Once the combustion reaction started, the fire starts from the surface and extends to the interior.[18] After complete combustion, the obtained foamy black powder was ground well using mortar and pestle. Finally, NFO powder was sintered at its own phase formation temperature for 3h (Scheme 1). The obtained product was confirmed by XRD.

C. Preparation of $NiFe_2O_4$/polypyrrole core–shell

The polymerization of pyrrole was carried out by a chemical oxidative reaction with NFO material at 0–5°C. The specified amount of above prepared NFO was dispersed in a separate beaker containing 100 ml of 0.01 M SDS as a surfactant (Table I). Subsequently, double distilled but cooled liquid pyrrole (0.1M) was added to each suspension containing beaker under rigorous stirring (1800 rpm). An aqueous solution of $FeCl_3$ which is act as oxidizing agent was gradually added in to each suspension. The rigorous stirring was carried out for 8 h. The two separate layers were observed. Light weight upper layer consist of only PPy was removed by decantation. Bottom dens layer consist of PPy coated NFO particles was filtered, washed with 50:50 distilled water/ethanol solvent and dried at 60°C for 24 h in the oven.

D. Supercapacitor fabrication and measurements

Pure PPy, NFO and NFO/PPy composite electrodes were prepared by using a hydraulic pellet press machine. High pressure (10 ton) was applied to the compositepowder to obtain a hard-round pellet electrode (1.5cm diameter, 2mm breadth). Poly (ethylene oxide) was used as electrolyte separator to form sandwich-type construction (electrode/separator/electrode) between two pellets with a silver paste current collector to form two-electrode capacitor cells. The electrodes were pre wetted with electrolyte before use. The performance of capacitor was observed by using galvanostatic charge–discharge method at room temperature.

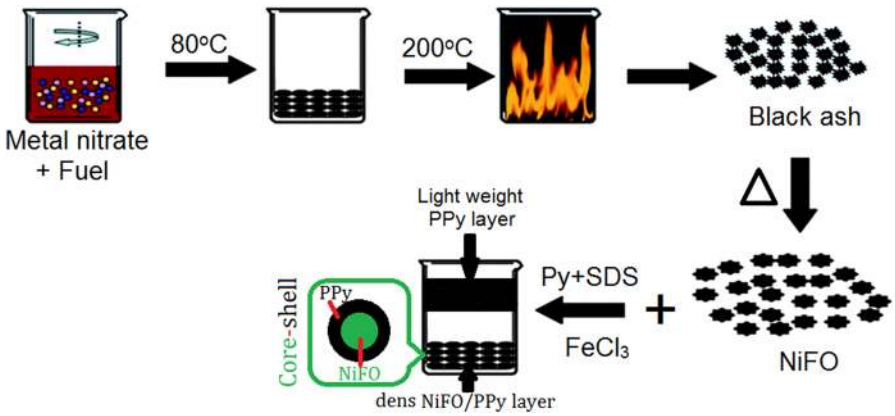

SCHEME 1. Schematic representation of Synthesis of NFO and NFO/PPy core-shell composite material.

TABLE I. Composition and labeling of composite materials.

Designation	NFO (%)	NFO/PPy (%/%) Dense layer	PPy (%) Floating layer
PPy	00	00	100
NFO/PPy1	10	10/20	80
NFO/PPy2	20	20/40	60
NFO/PPy3	30	30/60	40
NFO/PPy4	40	40/80	20
NFO/PPy5	50	50/100	00
NFO/PPy6	60	(50/100) +10%NFO	00
NFO/PPy7	70	(50/100) +20%NFO	00

III. RESULTS AND DISCUSSION

A. FT–IR analysis

The FT–IR spectra of PPy, NFO and polypyrrole coated NFO core–shell material measured using their powder are shown in Figure 1. The characteristic absorption bands of polypyrrole are observed at 785, 923, 1043, 1170, 1393, 1552, 1640, 3439, 3749 and 3853 cm^{-1}.[19] The absorption peaks at 788, 1051, 1393, 1552, 1640, 3439, 3749 and 3853cm^{-1} were existing in NFO/PPy core–shell, due to the interaction of ferrite and polypyrrole backbone. The C–H wagging vibration at 788 cm^{-1}, =C–H out-of-plane vibrations at 923 cm^{-1}, C–H in plane deformation at 1043 cm^{-1} and C–N stretching vibration at 1170 cm^{-1} were observed in PPy as well as NFO/PPy. The IR peak obtained at 1043 and 923 cm^{-1} are due to the =C–H out of plane vibration indicating the polymerization of pyrrole. The characteristic peaks at 1552 cm^{-1} and 1464 cm^{-1} correspond to the C=C stretching, whereas peaks at 1314 cm^{-1} represent to C–N bonds. The N–H and C–H stretching vibration of polypyrrole appeared at 3439 and 2929 cm^{-1} respectively.[20] The major peaks observed in the ferrite materials as well as polypyrrole match well with its core–shell confirming the formation of NFO/PPy material. The shifting as well as disappearance of some absorption peaks is due to formation of core–shell. Finally, all fundamental bands of NFO as well as PPy are observed in its NFO/PPy core–shell structure are confirming the formation of NFO/PPy composite material.

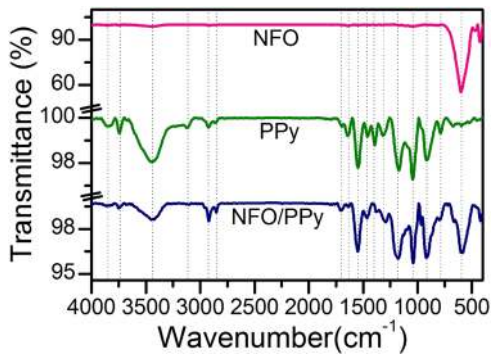

FIG. 1. FT–IR spectrum of NFO, PPy and NFO/PPy composites.

B. SEM and EDS analysis

In present work, the morphology of ferrite and PPy coated ferrite core–shell materials are shown in Figure 2. Images (a, b, c) are the micrographs of the NFO, PPy, NFO/PPy. Image (d) is FE-TEM of the NFO/PPy core-shell and image (e, f) represents EDS spectrum and elemental composition of NFO/PPy composite. NFO prepared from sol gel auto combustion root was confirmed by SEM image (a). It has non uniform trigonal pyramidal structure and close to each other. The diameter of the trigonal pyramidal particles is varying from 100 nm to 300 nm. Pure PPy and NFO/PPy nanoparticles are porous but agglomerated to each other (b, c). The porous agglomerated particles have the tendency to form a number of nano globules and each globule consist of a number of compacted nanoparticles. These globules are around 100 to 200 nm in range. An elemental composition of NFO/PPy composite was determined by EDS. The major elements in the NFO/PPy composite were carbon and oxygen, iron and nickel. Carbon, nitrogen and oxygen are primarily associated with PPy while other are related to ferrite (f). The SEM-EDS analysis revealed the formation of NFO/PPy composite material.

C. XRD analysis

X-ray diffraction pattern for NFO and NFO/PPy core–shell structures are shown in Figure 3. The broad peak of amorphous polypyrrole is due to the scattering from materials at interplanar spacing. The sharp diffraction peaks of NFO particles are observed at 30.24°, 35.79°, 37.37°, 43.40°, 54.01°, 57.49°, 63.04°, 71.60°, 74.61°, 75.72°, and 79.04° can be indexed as the (220), (311), (222), (400), (422), (511), (440), (620), (533), (622) and (444) planes of crystalline structure. It can be clearly indexed to face centered cubic (fcc)[21] structure of NFO [JCPDS Card No. 10-0325]. However, all peaks of NFO/PPy core–shell are broad at base but exact similar with respect to their NFO material. The PPy should display characteristic broad peak at 24°–27° 2θ value.[22] Sometime, the characteristic peak of PPy was covered with that of NFO/PPy core–shell. Therefore, we cannot observe this characteristic peak of PPy in core–shell composite. Thus, XRD pattern provides an additional evidence of the interaction between polymer and the NFO particles. In case of NFO particles, the intensity of diffracted peaks is high due to the less absorption and more diffraction occurs in X-ray beam by crystalline ferrite particles. Above all nanocomposites, the intensity of peaks is decreased due to the polypyrrole shell. Hence more absorption and less diffraction of X-ray beam is taking place which demonstrates that the formation of NFO/PPy core–shell structures.

D. Electrical property

The temperature dependent electrical conductivity of NFO/PPy composites and electrical conductivity as a function of different Wt% loadings of NFO is represent in Figure 4(a, b). The electrical conductivities of PPy and NFO/PPy composites in the form of pressed electrodes were determined using four-point probe set–up system and Keithley digital multimeter. Electrical conductivity of pristine PPy was found to be 9.9Scm^{-1} at 28°C. However, NFO/PPy composite shows a higher value of conductivity. The electrical conductivity of the core–shell composites increases relatively with the

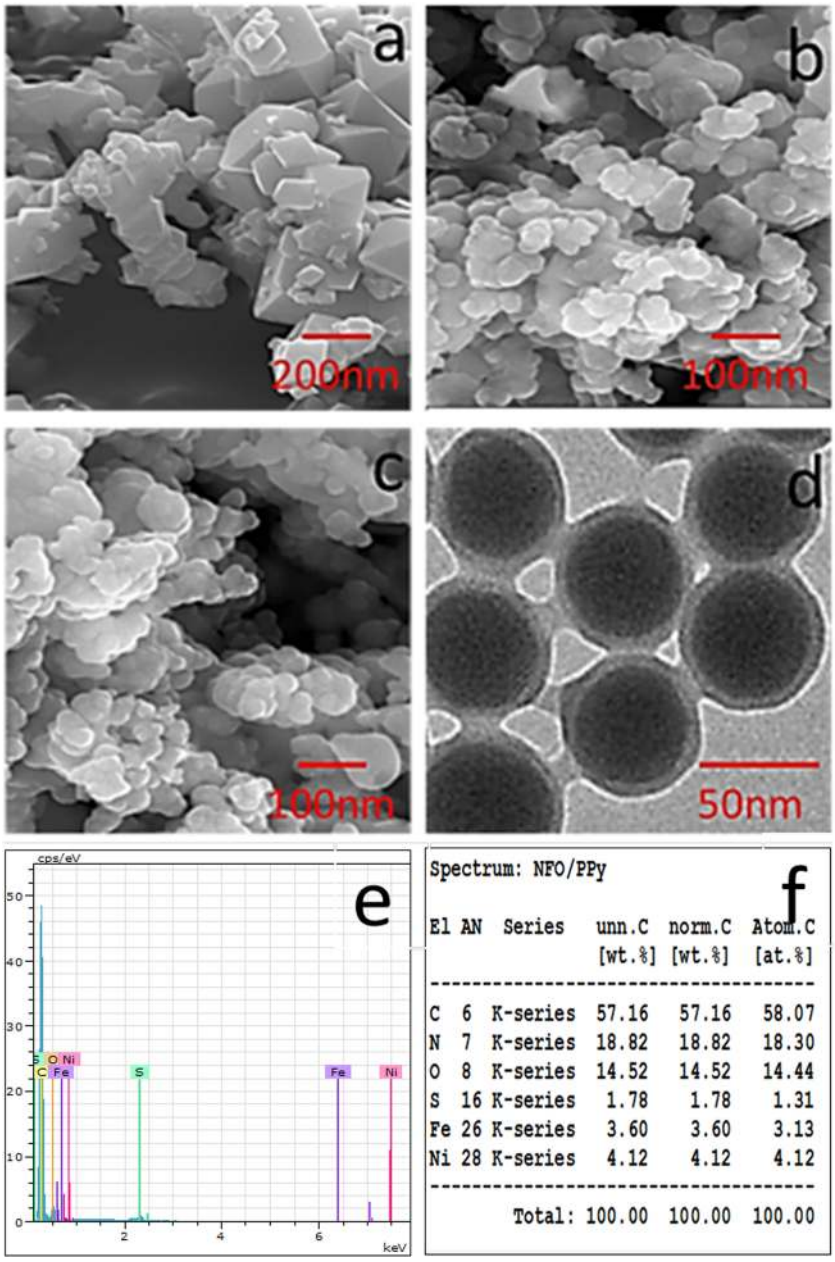

FIG. 2. SEM image of NFO (a), PPy (b), NFO/PPy (c); TEM of NFO/PPy (d) and EDS of NFO/PPy (e, f).

increasing weight % of ferrite loading. The maximum value of electrical conductivity was observed at 50 weight % of NFO materials loading (b). It was observed that the conductivity of NFO/PPy material increases with the rising temperature which resembles to the semiconductor conductivity. Above 200°C, NFO/PPy material found to decompose easily with the rapid fall in conductivity. Therefore, conductivity measurements for these composites can be carried out up to 200°C. The change in conductivity is found in the order of NFO/PPy>PPy which is presented in (a). The large enhancement in electrical conductivity is observed which is in proportionate to the core and shell interface. The increased interface facilitates to form the large conductive network in the composite. The strong ferrite–PPy interactions promote the charge transfer across the interface in composites leading to the enhanced electrical conductivity. The observed maximum conductivity for the 50 weight % NFO loading is found to be 132 Scm^{-1} relative to the conductivity of PPy.

In synthesis of these composites, we had tried to prepare the composite with the loading of 60% and 70% NFO. We observed that in 60% and 70% loading of NFO, the entire PPy was coated on some

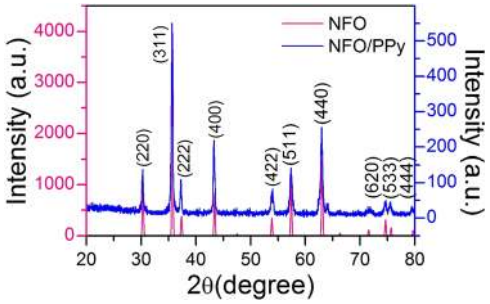

FIG. 3. XRD pattern of NFO and NFO/PPy composite.

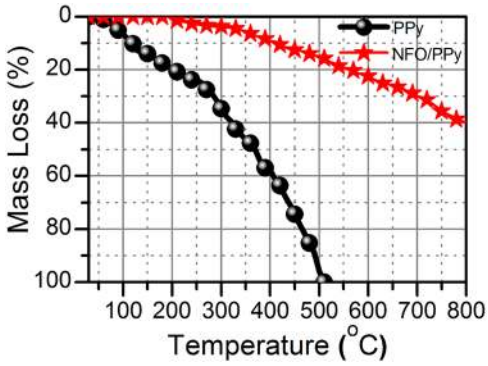

FIG. 5. Thermal gravimetric analysis of PPy and NFO/PPy composite.

part of NFO particles, but the rest particles remained uncoated at the bottom and the product contained core shell composite and additional uncoated NFO particles. These hybrid composite shows less conductivity as compared to core shell which we had tested already. Therefore, composites above 50% NFO loading did not displayed the expected increasing trend of conductivity. Due to this reason, we used 50% NFO loading core shell composite for application. If we increase molar concentration of pyrrole and oxidant, then excess of pyrrole will be utilized in the formation of coating on remaining NFO. Hence for 1M concentration, only 50% NFO loading is suitable for utilization of 100% PPy which give composite of possible high conductivity. Therefore, we used 50 weight % of NFO loading PPy for further characterization and applied as electrode material.

E. Thermal gravimetric property

The thermal behaviors of PPy and NFO/PPy core shell were studied using thermogravimetric analysis. The thermograms (Figure 5) show an unambiguous comparison between the thermal stability of selected conducting polymers and their nanocomposites in N2 atmosphere. In case of pristine PPy, PPy was found to be stable in the range of 30–80°C. Due to the traces of water or other impurities present in PPy, the initial decomposition take place around 80–260°C; 75% of the mass of PPy was preserved at 260°C. After 260°C, continuous, linear weight loss was observed up to 510°C and 100% mass loss was observed. It is proved that pure PPy has not much good thermal stability.

In case of NFO/PPy nanocomposite, NFO/PPy composite was found to be stable in the range of 30–250°C. The initial decomposition take place around 250°C due to the traces of water or other impurities present in the composites. Up to 1% of the mass loss of composites was observed at 250°C. After 250°C, the nanocomposites slowly undergo thermal degradation therefore, it shows the thermal stability decreased constantly from 250°C and continuous, linear weight loss observed up to 800°C. A composite shows 39% weight loss up to 800°C and all polypyrrole shell was found to be vanished at that temperature. The stability of NFO/PPy nanocomposite was found to be observed in the order of PPy < NFO/PPy respectively up to 800°C due to the presence of strong interaction between PPy chain and NFO.

F. Supercapacitive studies

The chemically synthesized pure PPy and NFO/PPy composite electrodes were used in electrochemical capacitors. Supercapacitive performance was tested by means of cyclic voltammetry and galvanostatic charge–discharge techniques.

G. Cyclic voltammetric analysis

Cyclic voltammetry was carried out using a three–electrode system. Pure PPy or NFO or NFO/PPy composite electrode, standard calomel electrode (SCE) and Pt electrode were used as working electrodes, reference electrode and counter electrode respectively. 1M H_2SO_4 solution was used as aqueous electrolyte. The potential window was kept constant and scan rate was varied as; 10, 20, 30, 50 and 100mVs^{-1}. The measurements were calibrated using ferrocene as the standard at a scan rate of 10mVs^{-1}. Figure 6(a, b) shows the cyclic voltammograms of pure polypyrrole and NFO/PPy for variable scan rates. The oxidation reduction peaks are observed in both

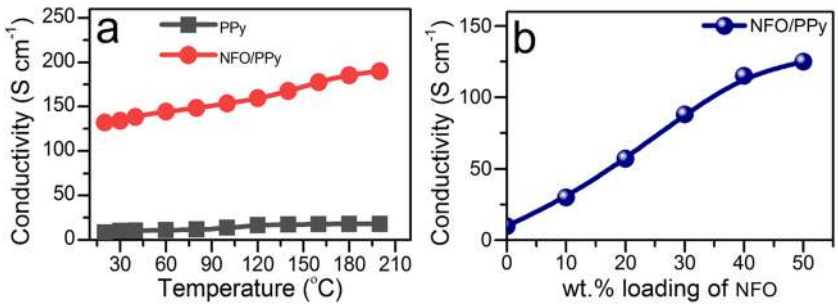

FIG. 4. Temperature dependent conductivity of PPy and NFO/PPy (a), electrical conductivity as a function of different wt % loading of NFO (b).

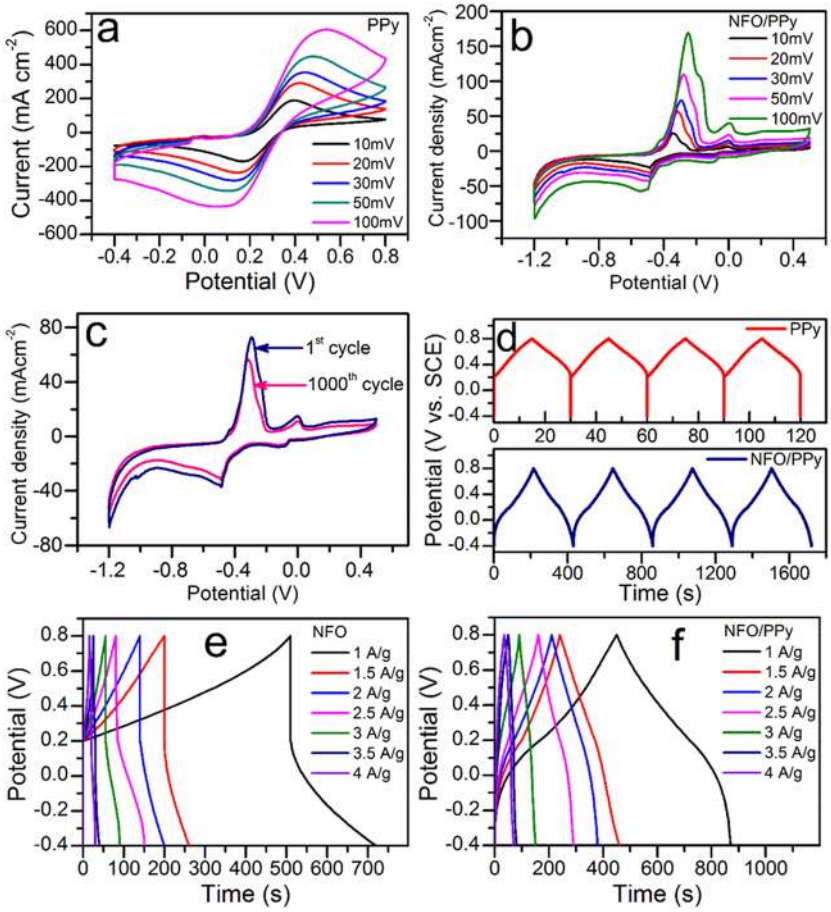

FIG. 6. The CV curves of (a) PPy and NFO/PPy (b). The CV curves of NFO/PPy at 1st and 1000th cycles (c). Repeated charge discharge pattern of PPy and NFO/PPy (d). The charge discharge curves of NFO (e) and NFO/PPy (f).

pure PPy as well as NFO/PPy nanocomposite. $Ni^{2+/3+}$ and/or $Fe^{3+/2+}$ transition metal ions undergo facile redox reactions to form oxidation reduction peaks which were observed in the CV. These redox peaks are responsible for pseudocapacitive behavior of NFO electrode. As scan rate increases from 10-100 mVs^{-1}, the shape of the CV curve does not change like rectangular shape. This is due to the strong interaction between the electrolyte and the electrode surface. At low scan rates, ions have sufficient time to diffuse into the electrode material and utilize all of the available active sites of electrode. But at the high scan rates, only surface species of electrode can participate in the electrochemical process. NFO/PPy electrode shows large integrated area, which indicates the admirable electrochemical concert and large active surface area for charge storage as compared to pure PPy electrode.

Figure 6(a) shows redox peaks of pure PPy thin electrode within the potential window from –0.4 to +0.8 V versus SCE with variable scan rates of 10–100mVs^{-1}. The CV shows the oxidation peaks at +0.38, +0.41, +0.44, +0.48 and +0.53V for 10–100mVs^{-1} versus SCE, which are attributed to the oxidation of polypyrrole back bone. In the reverse scan the reduction peaks are observed at +0.17, +0.14, +0.13, +0.10 and +0.07V versus SCE, which are attributed to the reduction of polypyrrole backbone. As compared to the reverse scan, the current densities were increased during oxidation process of polypyrrole which may be due to the insertion of SO_4^{2-} ions into polymer chain. Figure 6(b) shows redox peaks of NFO/PPy electrode within the potential window from –1.2 to +0.5 V versus SCE with variable scan rates of 10–100mVs^{-1}. The slightly shifting of the oxidation and reduction potentials was observed for NFO/PPy electrode. The oxidation peaks are observed at –0.34, –0.31, –0.29, –0.27 and –0.24V for 10–100mVs^{-1} versus SCE, which are attributed to the oxidation of NFO/PPy composite. In the reverse scan the reduction peaks are observed at –0.49, –0.49, –0.49, –0.49 and –0.53V versus SCE, which are attributed to the reduction of NFO/PPy composite. As compared to the reverse scan, the current densities were increased during oxidation process of NFO/PPy electrode which may be due to the insertion of SO_4^{2-} ions into NFO/PPy composite. The interfacial and specific capacitance decreases with increase in scan rate. The inner active sites cannot sustain the redox transitions completely due to the diffusion effect of protons within the electrode. From Figure 6(a, b), it is observed that all redox peaks which implies the current–potential behavior as a function of voltage. The redox reactions of PPy chain with electrolyte are responsible for supercapacitive performance.

H. Stability of NFO/PPy electrode

The electrochemical stability of core–shell electrode in 1M H_2SO_4 was tested by cyclic voltammetry method. Figure 6(c) shows the typical C–V curves for 1st and 1000th cycles and Figure 6(d) shows the repeatability of PPy and NFO/PPy electrodes. The current under curve is decreased by 2.76% up to 1000 cycles. The long-lasting stability and the repeatability of electrode material are considered for the selection of its supercapacitor applications. There is no significant decrease in specific capacitance observed during 1st cycle to 1000th cycle which indicates the excellent electrochemical stability of NFO/PPy composite electrode over a large number of cycle operations in energy storage application. The specific and interfacial capacitances are found to decrease in small amount up to 1000th cycle because of the small loss of active material.

I. Galvanostatic charge–discharge (GCD) study

Galvanostatic charge–discharge study of pure PPy, NFO and NFO/PPy electrode are carried out at different current density. The characteristic charge–discharge curves of electrodes in 1M H_2SO_4 electrolyte at −0.4 to +0.8 V/SCE is shown in Figure 6(e, f). It is observed that, almost all discharging curves of PPy and NFO electrode exhibit ideal linear curve, which point out the pseudocapacitive behavior. But in case of NFO/PPy electrode, discharging curves are not perfect straight lines. Therefore, the process of a Faradaic reaction occurs. Hence, it shows supercapacitive property. Internal resistance is most important and it is responsible for the initial potential drop. The internal resistance which depends on the surface morphology of electrode is due to the presence of interfacial contact resistance between electrodes and 1M H_2SO_4 electrolyte. Due to the NFO loading, the interaction between ferrites and PPy in the polymer matrix are responsible for significant changes in the morphology of composite electrodes. However, the resistance of supercapacitor is decreased because of the generation of a large electrode/electrolyte contact surface area due to the various morphologies of electrode. The discharging time of electrodes increases in the order of PPy < NFO < NFO/PPy. This feature may be attributed to the increased conductivity of NFO/PPy electrodes, which facilitates the fast charge transport in the composite electrode.

The supercapacitive parameters such as values of specific capacitance (C_s), specific energy (E_s), specific power (P_s) and coulombic efficiency (η%) for PPy, NFO and NFO/PPy electrodes were estimated from the discharge process according to the following equation:[23]

$$Specific\ capacitance\ C_s = \frac{I_d \times T_d}{\Delta V \times W} \quad (1)$$

$$Specific\ energy\ E_s = \frac{C_s \times \Delta V^2}{2} \quad (2)$$

$$Specific\ power\ P_s = \frac{E_s^2}{T_d} \quad (3)$$

$$coulombic\ efficiency\ \eta\% = \frac{T_d}{T_c} * 100 \quad (4)$$

TABLE II. Specific capacitance, specific energy, specific power and columbic efficiency for electrodes at constant current density of $1Ag^{-1}$.

Electrodes	Specific capacitance (Fg^{-1})	Specific energy ($Wh\ Kg^{-1}$)	Specific power ($kW\ Kg^{-1}$)	Columbic efficiency (η%)
PPy	624.17	44.94	13.4	98.13
NFO	507.21	36.51	4.98	42.45
NFO/PPy	721.66	51.95	6.18	99.08

Where I_d is the discharge current, T_d is the discharge time; ΔV is the potential change during discharge process (potential window) and W is the mass of active material. The variation of specific capacitance (Fg^{-1}), specific energy ($Wh\ kg^{-1}$), specific power ($kW\ kg^{-1}$) and coulombic efficiency (η %) obtained for electrodes at $1Ag^{-1}$ are shown in Table II. The specific capacitance obtained from CV and GCD techniques are comparable. Further, specific capacitance, specific energy, specific power and coulombic efficiency of NFO/PPy electrodes are greater as compared to other one. Therefore, it is confirmed that the NFO/PPy electrode shows improved supercapacitive performance than pure PPy and NFO electrode.

J. Electrochemical impedance spectroscopy

The capacitive behavior of NFO/PPy electrode for supercapacitor is also determined with the help of electrochemical impedance spectroscopy. Figure 7 represents the nyquist plot of NFO/PPy material over 40Hz-20MHz frequency range. The nyquist plot shows semicircle curve in the high frequency region. The point at which the curve creates an intercept on the real axis which gives the solution resistance or equivalent series resistance (R_s = 9.4 Ω) of the electroactive material. The vertical line was not found to be observed in the low frequency region and highest peak of semicircle is present in high frequency region. This indicates the supercapacitive behavior of NFO/PPy electrode.

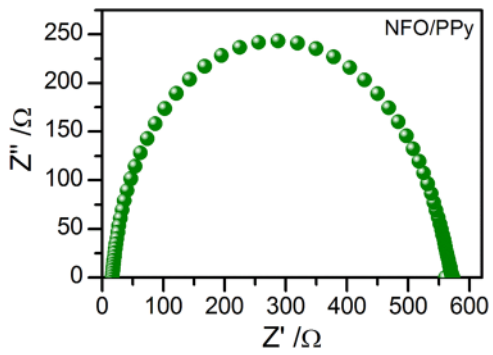

FIG. 7. Electrochemical impedance spectrum (Nyquist plot) of NFO/PPy.

IV. CONCLUSIONS

The simple cubic spinel ferrite based polypyrrole core–shell materials are successfully synthesized by *in situ* polymerization of pyrrole in the presence of ready NFO particles. The interaction between NFO materials and PPy in their nanocomposites was confirmed by FT–IR studies. SEM studies revealed that the prepared NFO/PPy composite shows uniformly porous and agglomerated globular morphology. The X–ray diffraction pattern of NFO/PPy composite showed the highly intense but broad base peaks indicating the nano crystallinity of the composites. This is due to the presence of strong interaction of ferrite materials with pristine PPy chain. Thermal analysis showed that, the incorporated NFO material boosts the thermal stability of core shell composite as compared to pure PPy. This is evidenced to the strong interaction between ferrite and pristine PPy chain. The conductivity of NFO/PPy composite increases as a function of temperature which is attributed to the semiconductor behavior. The weight % loading of NFO into the PPy matrix during the synthesis leads to boost the electrical network. Therefore, higher electrical conductivity of composites is observed at 50 weight % loading of NFO ferrite as compared to pure PPy. The specific capacitance, specific energy, specific power and columbic efficiency of NFO/PPy electrode are found to be enhanced as compared to the pure PPy. Hence, it is confirmed that the core–shell material electrode shows the improved supercapacitive performance than the pure PPy as well as NFO electrodes.

ACKNOWLEDGMENTS

Authors are thankful to the Department of Applied Science, College of Engineering, Pune and Department of Physics, Indian Institute of Science, Bangalore, India for providing the research facilities. Also, authors are thankful to AICTE for the support of small contingency grant for student, New Delhi, India.

REFERENCES

[1] X. Liu and P. G. Pickup, "Performance and low temperature behaviour of hydrous ruthenium oxide supercapacitors with improved power densities," Energy Environ. Sci. **1**(4), 494–500 (2008).
[2] S. G. Kandalkar, D. S. Dhawale, C. K. Kim, and C. D. Lokhande, "Chemical synthesis of cobalt oxide thin film electrode for supercapacitor application," Synth. Met. **160**(11-12), 1299–1302 (2010).
[3] A. Sardar and P. S. Gupta, "Polypyrrole based nanocomposites for supercapacitor applications: A review," AIP Conf. Proc. **1953**, 030020 (2018).
[4] C. N. Chinnasamy *et al.*, "Mixed spinel structure in nanocrystalline $NiFe_2O_4$," Phys. Rev. B - Condens. Matter Mater. Phys. **63**(18), 184108 (2001).
[5] P. Sivakumar, R. Ramesh, A. Ramanand, S. Ponnusamy, and C. Muthamizhchelvan, "Synthesis and characterization of $NiFe_2O_4$ nanoparticles and nanorods," J. Alloys Compd. **563**, 6–11 (2013).
[6] A. Ahlawat, V. G. Sathe, V. R. Reddy, and A. Gupta, "Mossbauer, Raman and x-ray diffraction studies of superparamagnetic $NiFe_2O_4$ nanoparticles prepared by solgel auto-combustion method," J. Magn. Magn. Mater. **323**(15), 2049–2054 (2011).
[7] Z. Wang, Y. Yang, D. L. Olmsted, M. Asta, and B. B. Laird, "Evaluation of the constant potential method in simulating electric double-layer capacitors," J. Chem. Phys. **141**(18), 184102 (2014).
[8] L. L. Zhang and X. S. Zhao, "Carbon-based materials as supercapacitor electrodes," Chem. Soc. Rev. **38**(9), 2520–2531 (2009).
[9] S. Sinha, "Spatiotemporal consequences of random coupling," Proc. Indian Natl. Sci. Acad. Part A - Phys. Sci. **71**(1-2), 97–111 (2005).
[10] Y. Jang, J. Jo, H. Jang, I. Kim, D. Kang, and K. Y. Kim, "Activated carbon/manganese dioxide hybrid electrodes for high performance thin film supercapacitors," Appl. Phys. Lett. **104**(24), 243901 (2014).
[11] C.-C. Hu and C.-Y. Cheng, "Ideally pseudocapacitive behavior of amorphous hydrous cobalt-nickel oxide prepared by anodic deposition," Electrochem. Solid-State Lett. **5**(3), A43 (2002).
[12] S. Kuo and N. Wu, "Study on ferrites for supercapacitor application," *56th Annu. Meet. Int. Soc. Electrochem.*, no. December, pp. 1–5, 2015.
[13] P. Bhojane, A. Sharma, M. Pusty, Y. Kumar, S. Sen, and P. Shirage, "Synthesis of ammonia-assisted porous nickel ferrite ($NiFe_2O_4$) nanostructures as an electrode material for supercapacitors," J. Nanosci. Nanotechnol. **17**(2), 1387–1392 (2017).
[14] V. Venkatachalam and R. Jayavel, "Synthesis of Co_3O_4 electrode material for supercapacitor applications," Int. J. ChemTech Res. **6**(13), 5404–5407 (2014).
[15] K. Hareesh *et al.*, "PEDOT:PSS wrapped $NiFe_2O_4$/rGO tertiary nanocomposite for the super-capacitor applications," Electrochimica Acta **201**, 106–116 (2016).
[16] P. Sahoo, R. G. Shrestha, L. K. Shrestha, J. P. Hill, T. Takei, and K. Ariga, "Surface oxidized carbon nanotubes unformly coated with nickel ferrite nanoparticles," J. Inorg. Organomet. Polym. Mater. **26**(6), 1301–1308 (2016).
[17] M. Oguntoye, S. Oak, L. Pashazanusi, L. Pratt, and N. S. Pesika, "Vertically-aligned carbon nanotube arrays as binder-free supports for nickel cobaltite based Faradaic supercapacitor electrodes," Electrochim. Acta **236**, 408–416 (2017).
[18] L. Sun, R. Zhang, Z. Wang, L. Ju, E. Cao, and Y. Zhang, "Structural, dielectric and magnetic properties of $NiFe_2O_4$ prepared via sol–gel auto-combustion method," J. Magn. Magn. Mater. **421**, 65–70 (2017).
[19] M. A. Chougule, S. G. Pawar, P. R. Godse, R. N. Mulik, S. Sen, and V. B. Patil, "Synthesis and characterization of polypyrrole (PPy) thin films," Soft Nanosci. Lett. **01**(01), 6–10 (2011).
[20] H. Kato, O. Nishikawa, T. Matsui, S. Honma, and H. Kokado, "Fourier transform infrared spectroscopy study of conducting polymer polypyrrole: Higher order structure of electrochemically synthesized film," J. Phys. Chem. **95**(15), 6014–6016 (1991).
[21] R. B. Kamble and V. L. Mathe, "Nanocrystalline nickel ferrite thick film as an efficient gas sensor at room temperature," Sensors Actuators, B Chem. **131**(1), 205–209 (2008).
[22] S. Shrikrushna, J. A. Kher, and M. V. Kulkarni, "Influence of dodecylbenzene sulfonic acid doping on structural, morphological, electrical and optical properties on polypyrrole/3C-SiC nanocomposites," J. Nanomed. Nanotechnol. **06**(05), 313 (2015).
[23] P. M. Kharade, J. V. Thombare, A. R. Babar, R. N. Bulakhe, S. B. Kulkarni, and D. J. Salunkhe, "Electrodeposited nanoflakes like hydrophilic Co_3O_4 as a supercapacitor electrode," J. Phys. Chem. Solids **120**(September), 207–210 (2018).